Electronic Supplementary Information for

"UV-Visible photo-reactivity of permanently polarized inorganic nanotubes coupled to gold nanoparticles"

Sabyasachi Patra[a,b,*], Fabienne Testard[a], Frédéric Gobeaux[a], Lorette Sicard[c], Delphine Shaming[c], Sophie Le Caër[a,*], Antoine Thill[a,*]

[a]Université Paris-Saclay, CEA, CNRS, NIMBE, 91191, Gif-sur-Yvette, France

[b]Radiochemistry Division, Bhabha Atomic Research Centre, Trombay, Mumbai - 400085, India

[c]Université de Paris, ITODYS, CNRS, UMR 7086, 15 rue J.-A. de Baïf, F-75013, Paris, France

*E-mail: spatra@barc.gov.in, sspatra86@gmail.com, sophie.le-caer@cea.fr, antoine.thill@cea.fr

1. Cryo-TEM images showing the morphology of pristine Imo-CH_3 NTs after dialysis

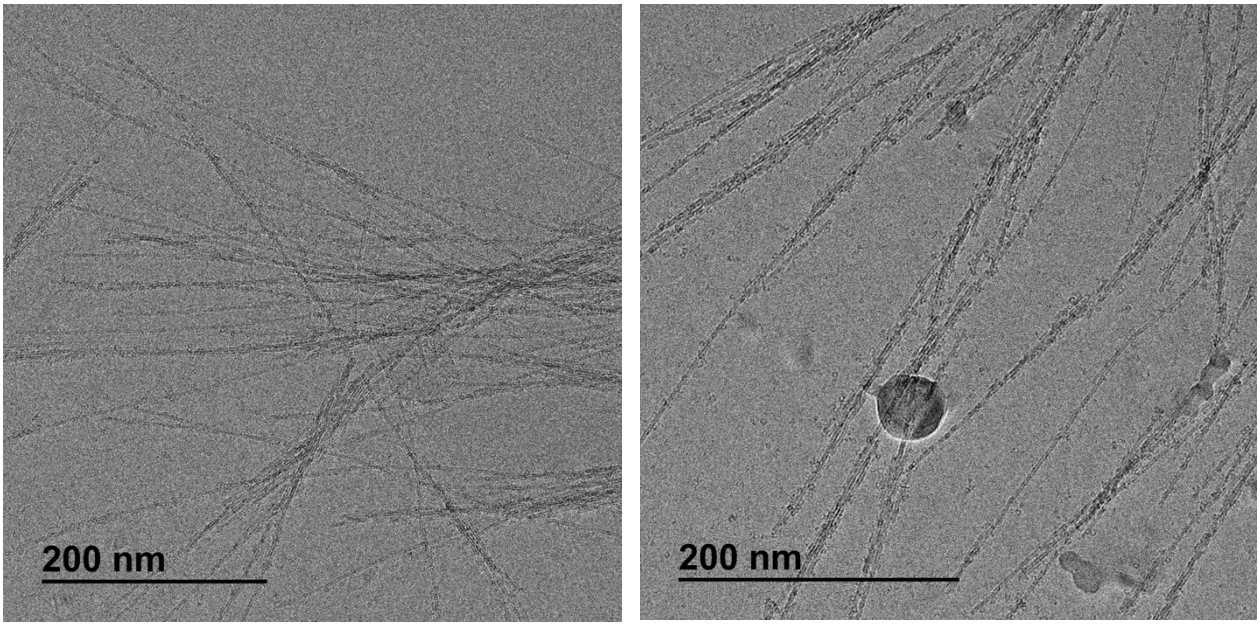

Figure S1. *Cryo-TEM images of pristine Imo-CH_3 NTs.*

2. SAXS data of pristine Imo-CH_3

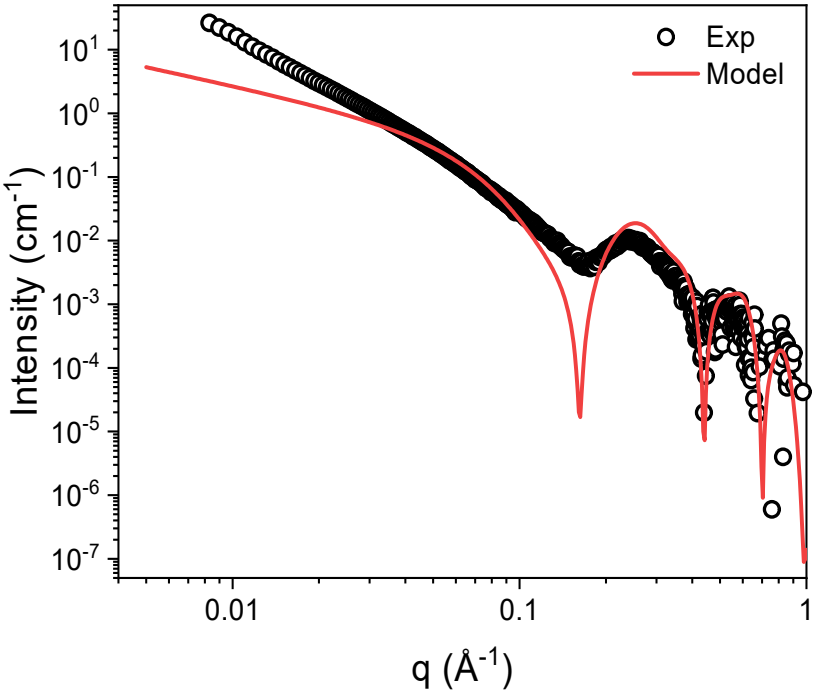

Figure S2. *SAXS profile of pristine Imo-CH_3 (circles) and the simulated SAXS profile (red line). In the low q range, the excess scattering signal results from interactions between imogolite NTs or aggregations of imogolite NTs.*

Table S1. *Parameters for the simulated SAXS profile of pristine Imo-CH_3*

	Imo-CH_3
Tube concentration (*N*: tubes/cm^3)	5.4×10^{14}
Inner radius (Å)	9.3
Wall thickness (Å)	6.0
Imogolite length (Å)	3500
Number of Si/ring	16
Number of atoms/structural unit	100
Lattice parameter (Å)	4.3
Internal electronic density (e.Å^{-3})	0.110
External electronic density (e.Å^{-3})	0.334
Number of 1 tube in bundles	2
Number of 2 tubes in bundles	0
Number of 3 tubes in bundles	2
Number of 4 tubes in bundles	1

3. SAXS analysis of Solution-A

For Solution-A, after subtraction of the imogolite-water suspension contribution, the total scattering can be adjusted by a sum of two contributions with parameters reported in table S2:

- A first for core/shell cylinder with only gold and chloride in the shell whose typical signature is visible for q > 0.3 $Å^{-1}$.
- a second in the low q range for the fractal organization of the cylinders (the Guinier contribution of the scattering in the low q range is not considered due to the q_{min} cut off):

$$\frac{B}{q^p} \times \left[1 - erf\left(\frac{qR_g}{\sqrt{6}}\right)^2\right]_+ \mathrm{b_f}$$

With B the fractal amplitude, P the fractal slope, Rg a Guinier radius and b_f the background.

The size of the internal diameter of the gold shell is fixed by the external diameter of imogolite (3 nm). The number of imogolite is fixed by the weight composition of the sample (2.3 $mg.mL^{-1}$). The thickness of the shell of the SAXS model was then adjusted to 0.67 nm (imposing the value of the scattering length density (SLD) of the shell) in order to properly fit the experimental SAXS pattern.

Table S2. *Parameters used to simulate the SAXS profile of Solution-A subtracted with pristine Imo-CH_3. Simulation consists of a fractal organization of imogolite surrounded by gold (core/shell model).*

	Simulation parameters	
Core/shell cylinder	Tube concentration (*N* : tubes.cm^{-3})	5.4×10^{14}
	Inner diameter (nm)	3.06
	Outer diameter (nm)	4.4
	length (nm)	350
	*SLD of cylinder core (cm^{-2})	0
	SLD of cylinder shell (cm^{-2})	1.9×10^{10}
	SLD of medium (cm^{-2})	0
Fractal organization	P (fractal slope)	2.1
	B (fractal amplitude)	0.001
	R_g (nm)	6.0
	b_f	0.012

*SLD: scattering length density

4. XPS Cl 2p photoelectron core-level spectrum of Solution-A

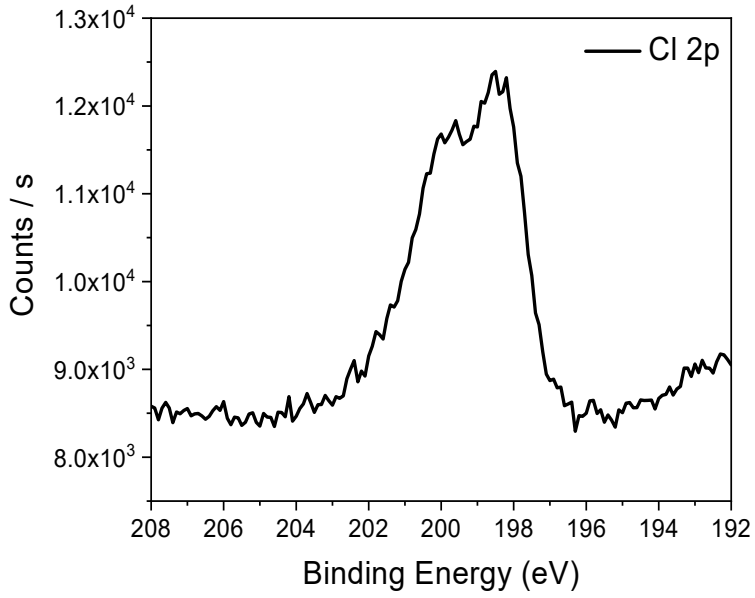

Figure S3. *Cl 2p photoelectron core-level spectrum of Solution-A.*

5. Photo-reduction of gold in the presence of Imo-CH_3 NTs in an aqueous medium

To unravel the participation of Imo-CH_3 photoelectrons in the reduction of gold ions, control experiments were performed at acidic pH in the absence and presence of Imo-CH_3 nanotubes (pH = 2.4, Figure S4a and S4b, respectively) without addition of propan-2-ol. The study was performed at acidic pH in order to be able to follow the reduction of Au(III) ions using UV-Vis spectroscopy (as $HAuCl_4$ solution shows an intense absorption around 300 nm at acidic pH). Propan-2-ol was not added to eliminate any source of electrons from direct photolysis of propan-2-ol so as to verify the photocatalytic role of Imo-CH_3 NTs in the reduction reaction. Comparison of both figures shows that reduction of Au(III) ions under UV illumination (time resolved decrease in absorbance at ~300 nm region) is highly facilitated in the presence of Imo-CH_3 NTs. Thus Imo-CH_3 is necessary for the formation of GNPs. This can only be explained by means of the Imo-CH_3-mediated photocatalysis.

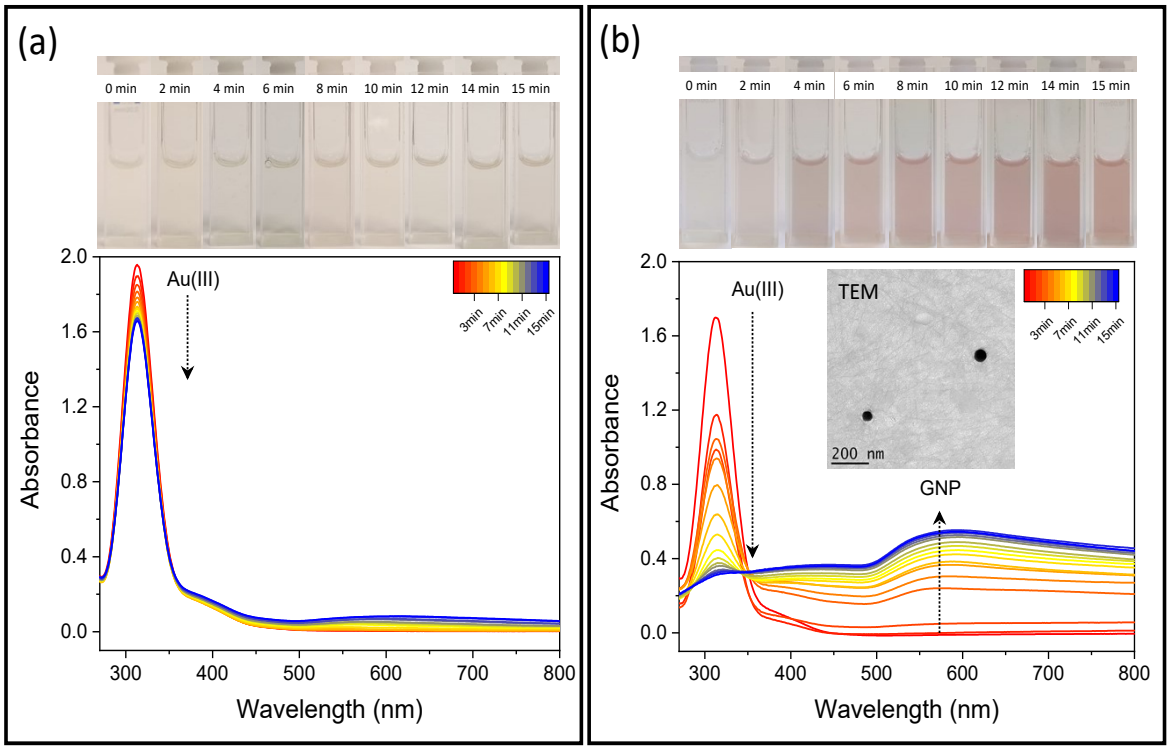

Figure S4. *Evolution of UV-Vis absorption spectra of $HAuCl_4$ aqueous solution (a) and $HAuCl_4$ – Imo-CH_3 mixed aqueous solution (b) during UV illumination under air atmosphere. The concentration of $HAuCl_4$ in both experiments is 0.34 mM. In experiment "b", imogolite is added to attain 1% w/w of gold per Imo-CH_3. The pH of the medium in all experiments was 2.4. Inset of "b" gives the TEM image of the sample at the end of UV illumination.*

6. SAXS profile of photolytically-produced GNPs

The SAXS patterns of the suspension after photolysis or radiolysis of *Solution-A* have been analyzed with a model of a Gaussian distribution of spheres together with fractal scattering in the lower q range and a contribution from core/shell cylinders of imogolite surrounded by gold atoms. Figures 2g in the main article shows the experimental SAXS patterns and the SAXS model adjusted on the experimental data. Table S3 summarizes the parameters used for the model.

Table S3. *Parameters for the simulated SAXS profile of photolytically produced GNP-coupled Imo-CH_3 NTs subtracted with pristine Imo-CH_3/water suspension scattering contribution (shown in Figure 2g). For more details on the parameters, see section 3 above.*

Photolytically produced GNPs-Imo-CH_3		
Gaussian sphere distribution	Sphere concentration (N: part.cm^{-3})	1.0×10^{13}
	Mean diameter (nm)	9.5
	Polydispersity	2
	SLD of spheres (cm^{-2})	1.31×10^{12}
	SLD of medium (cm^{-2})	0
Fractal contribution	B amplitude	0.0045
	D fractal slope	1.8
	R_g (nm)	8.0
	b_f	0.0004

The average GNP size, as obtained by SAXS analysis, is in agreement with the SEM/TEM analysis. Concerning the number of particles, SAXS analysis led to a value of 1.0×10^{13} part.cm^{-3}, which corresponds to a volume fraction of 5.10×10^{-6}, a significantly smaller value than the expected one calculated from the ICP-MS Au composition (9.80×10^{-6}). This could

be attributed to the presence of small particles and clusters adsorbed on imogolite, resulting in a mass fractal organization visible in the low q range data. From the Porod invariant law (a general property of SAXS diagram),[1] the total gold volume fraction could be estimated. In a first approximation, gold is assumed to be only under the form of Au(0) with a SLD value of 1.31×10^{12} cm^{-2}. A value of 6.35×10^{-6} is then obtained. This value includes the contribution of gold sphere nanoparticles and of the gold attached on the imogolite wall (with an indirect contribution in the low q range as fractal organization). This value is also lower than the one expected from the ICP-MS composition (9.80×10^{-6}), but higher than the contribution of only AuNPs (5.10×10^{-6}). In the present case, the invariant is underestimated because of the restricted q_{min} and the missing scattering part from aggregates (i.e., no visible Guinier region in the low q range). From this order of range, we see that only a small fraction of gold is under the form of spheres of 9.5 ± 2.0 nm.

7. SAXS profile of radiolytically produced GNPs

The SAXS pattern issued from radiolytically-produced samples is slightly different from that issued from photolytically-produced samples. The SAXS pattern can be fitted by a Gaussian distribution of spheres. We retrieve in the low q range a mass fractal organization issued form the small clusters and particles adsorbed on imogolite. Figure 3f in the main article shows the experimental SAXS pattern and the SAXS model adjusted on the experimental data. The parameters for the model are summarized in Table S4.

Table S4. *Parameters for the simulated SAXS profile displayed in Figure 3f.*

Radiolytically produced GNPs-Imo-CH_3		
Gaussian sphere distribution	Sphere concentration (*N*: part.cm^{-3})	3.3×10^{13}
	Mean diameter (nm)	5.0
	Polydispersity	2.0
	SLD of spheres (cm^{-2})	1.31×10^{12}
	SLD of medium (cm^{-2})	0
Fractal contribution	*B* amplitude	0.02
	D fractal slope	1.6
	R_g (nm)	7.0
	b_f	0.0006

The volume fraction issued from spherical gold nanoparticles only (fitted by the double Gaussian distribution of spheres) is equal to 3.20×10^{-6}, while the volume fraction issued from the gold composition is equal to 9.80×10^{-6}. In this case also, gold could not be fully incorporated in the form of GNPs. A part of gold is missing, and is probably under small spherical particles or clusters adsorbed on the imogolites not detected by SAXS. As in the case of samples synthesized by the photolysis route, the Porod invariant law can be used to extract the gold volume fraction. Assuming that gold is only present as Au(0), the volume fraction is found to be 6.55×10^{-6}, a value still lower than the expected one. This corroborates that a fraction of gold exists in much smaller size than spheres of 5.0 ± 2.0 nm.

8. Stability of the GNP-Imo-CH_3 photocatalysts

In order to use the GNP-coupled Imo-CH_3 nanotubes as photoreactors, the stability of the nanotubes during thermal treatment in alkaline condition, photolytic/radiolytic treatment, after the formation of GNPs on the external surface and after multiple cycles of photocatalytic applications is important. A unique characteristic of the tubular morphology of Imo-CH_3 NTs is their ability to form self-supported thin films upon drying.[2] The Imo-CH_3 nanotubes coupled with

GNPs and after uses as photocatalyst also produce similar self-supported thin films upon drying. This suggests that the tubular morphology of Imo-CH_3 remains intact after coupling with GNPs by photolytic/radiolytic reduction.

In our previous work, the stability of Imo-CH_3 nanotubes during photocatalytic applications under UV light (253.7 nm, 4.15×10^{19} photons.$L^{-1}.s^{-1}$) was tested using UV-Vis and Fourier Transform Infrared (FT-IR) spectroscopy for upto 5 hours of UV illumination. The morphology and chemical structure of Imo-CH_3 photocatalysts were found to be extremely stable.[3] In this work, in order to detect any change in the chemical structure of the NTs after coupling with GNPs, both the pristine and GNP-coupled Imo-CH_3 NTs, were studied by FT-IR spectroscopy using a Bruker Tensor 27 Fourier Transform Infrared (FT-IR) spectrometer (Figure S5). 1 wt% of the sample was dispersed in high purity KBr, then pelletized into self-supporting discs using a pressure of 10^9 Pa. Spectra were then recorded from 100 scans in the 350-4000 cm^{-1} wavenumber range at a 2 cm^{-1} resolution. The KBr background was subtracted in all cases. Clearly, the FT-IR absorption spectra of pristine and GNP-coupled Imo-CH_3 NTs are similar. The presence of a doublet at 956/910 cm^{-1}, characteristic of the tubular structure of Imo-CH_3 due to Si-O-Al stretching and the band at 2980 cm^{-1}, characteristic of -CH_3 asymmetric stretching, suggests the good morphological integrity of Imo-CH_3 NTs under UV photolysis/gamma radiolysis and also in the presence of the surface-attached GNPs. The change in mutual intensity in the doublet (956/910 cm^{-1}) and the blue shift of the O-Al-O bending band (~ 419 cm^{-1} in pristine Imo-CH_3, ~423 cm^{-1} in GNP-coupled Imo-CH_3, together with a decrease in absorbance) are attributed to modifications in the local environment of Al due to the attachment of GNPs on the external surface of Imo-CH_3. Table S5 summarizes the assignment of FT-IR bands of pristine and GNPs decorated Imo-CH_3 NTs.

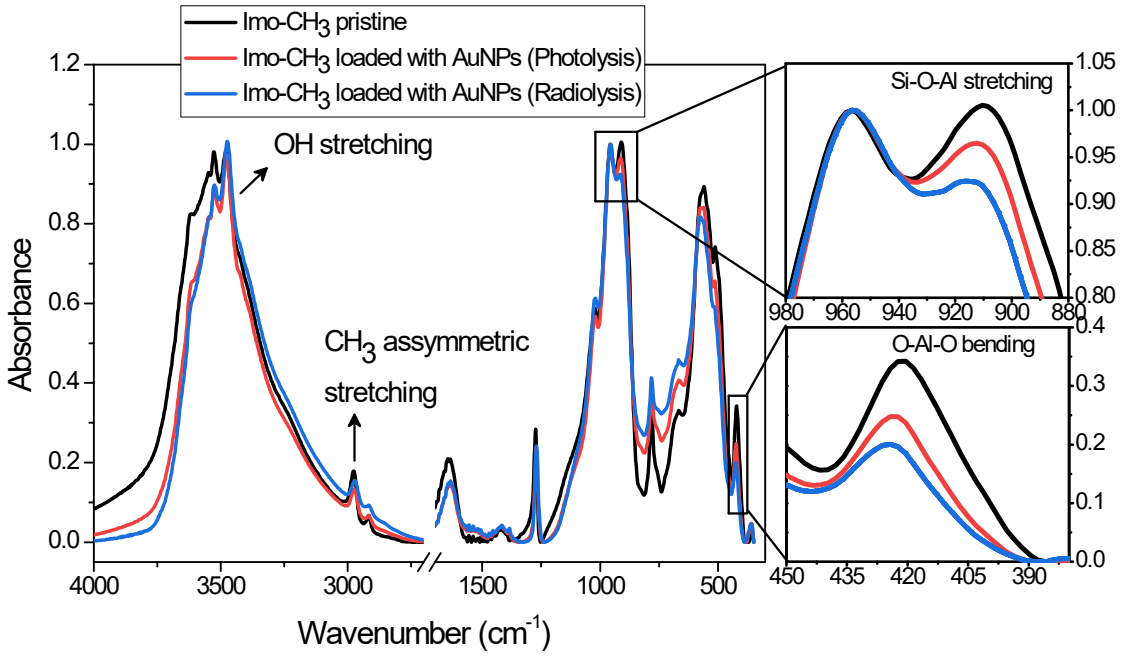

Figure S5. *FT-IR spectra of pristine (black curve) and GNP-coupled Imo-CH_3 NTs prepared by UV photolysis (red curve) and gamma radiolysis (blue curve) of Solution-A.*

Table S5. *Assignment of the vibrational bands of pristine and GNP-coupled Imo-CH_3 NTs.*

Assignment	**Wavenumber (cm^{-1})**		
		GNP-Imo-CH_3 prepared by	
	Imo-CH_3 pristine	**UV photolysis**	**Gamma radiolysis**
O-H stretching	4000-3000	4000-3000	4000-3000
CH_2/CH_3 asymmetric stretching	2980-2910	2980-2910	2980-2910
symmetric deformation of CH_3 in Si-CH_3	1273	1270	1270
Si-O-Al stretching	956/910	956/912	956/912
CH_3 rocking and Si-C stretching	782	782	782
Al-O modes	684, 570/548	684, 570/548	684, 570/548

O-Si-O bending	508	508	508
O-Al-O bending	419	423	423

In order to verify the stability of the surface coupled GNPs during the photocatalytic applications, UV-Vis spectrum of the GNP-Imo-CH_3 aqueous solution has been recorded after 9 repeated cycles of photocatalytic runs (1 hour of UV illumination, 253.7 nm, 4.15×10^{19} photons.L^{-1}.s^{-1}, in each cycle) and compared with the UV-Vis spectrum of the GNP-Imo-CH_3 systems before. For the photolytically-prepared GNP coupled Imo-CH_3 system, the UV-Vis spectrum of the solution changes minimally before and after photocatalytic applications (see Figure S6a), suggesting good stability of the photolytically prepared photocatalysts. On the contrary, the UV-Vis spectrum of the radiolytically-prepared sample slightly modifies after 9 cycles of photocatalytic application (see Figure S6b). This suggests that the morphology and/or concentration of the radiolytically synthesized GNPs on Imo-CH_3 surface slightly modifies upon prolonged illumination under UV light. The lower stability of the GNP-Imo-CH_3 photocatalyst, prepared by radiolytic route, is attributed to the weaker coupling of GNPs on the Imo-CH_3 surface. However, due to the stronger coupling of GNPs with the Imo-CH_3 surface in case of photolytically prepared system, the GNPs exhibits good stability over 9 photocatalytic cycles.

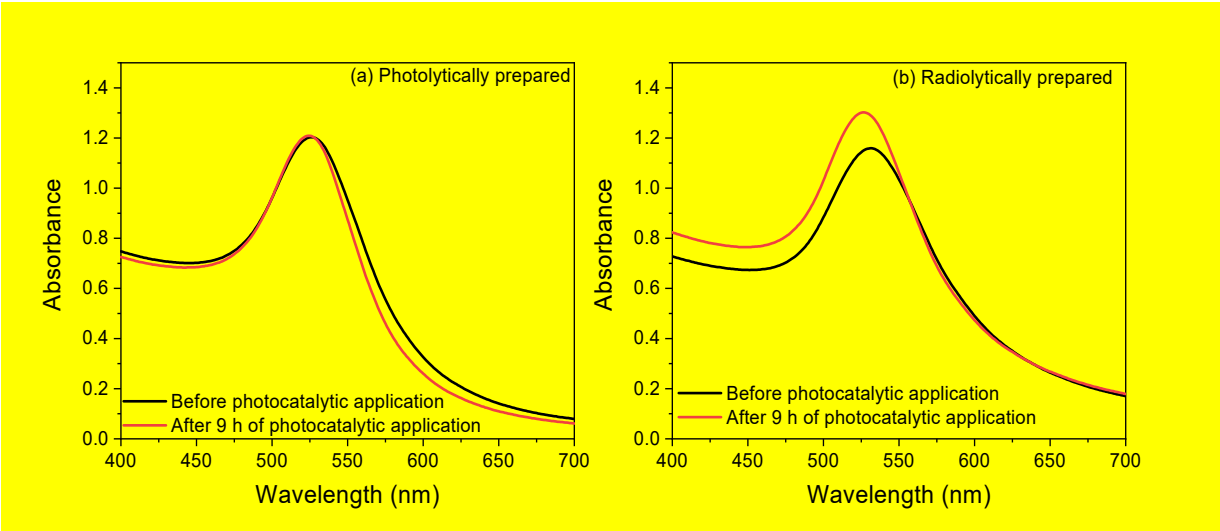

Figure S6. *UV-Vis spectrum of degassed aqueous solution of photolytically and radiolytically prepared GNP-Imo-CH_3 photocatalyst mixed with 20 vol% propan 2-ol before and after 9 cycles of photocatalytic H_2 production (1 hour illumination under UV light, 253.7 nm, 4.15×10^{19} photons.L^{-1}.s^{-1}, in each cycle).*

9. Redox balance model

We consider that among all photons involved in reaction R1, X µmol.g^{-1}.h^{-1} will lead to chemical reactions. As no net current is generated during this experiment, the quantity of e^- and of h^+ involved in these chemical reactions has to be balanced.

We make the hypothesis that the propan-2-ol and its degradation products are strongly confined inside the nanotubes. Therefore, as far as oxidation reactions are concerned, we will consider the two pathways (R1) and (R2) described in the main text as the only possible chemical pathways. We introduced the probability *p* for h^+ to be involved respectively in (R1), (*1-p*) being the probability of (R2).

$$C_3H_7OH + 18\ h^+ + 5\ H_2O \rightarrow 3\ CO_2 + 18\ H^+ \qquad (R1)$$

$C_3H_7OH + 10\ h^+ + 3\ H_2O \rightarrow 2\ CO_2 + CH_4 + 10\ H^+$ (R2)

For the reduction side (R3-R6), we consider the following chemical reactions with respective probabilities r_1, r_2, r_3 and $r_4$with $r_1 + r_2 + r_3 + r_4 = 1$.

$CO_2 + 8H^+ + 8e^- \rightarrow CH_4 + 2H_2O$ (R3)

$CO_2 + 2H^+ + 2e^- \rightarrow CO + H_2O$ (R4)

$2H^+ + 2e^- \rightarrow H_2$ (R5)

$Imo\text{-}CH_3 + e^- \rightarrow Imo\text{-}CH_3^-$ (R6)

If we write all these equations by taking into account their probabilities, we can obtain the balance for all possible species for a single e^- / h^+ pair.

$$\frac{p}{18}\,C_3H_7OH + p h^+ + \frac{5p}{18}H_2O \rightarrow \frac{3p}{18}CO_2 + pH^+$$

$$\frac{(1-p)}{10}\,C_3H_7OH + (1\text{-}p)h^+ + \frac{3(1-p)}{10}\,H_2O \rightarrow \frac{(1-p)}{5}\,CO_2 + \frac{(1-p)}{10}\,CH_4 + (1\text{-}p)H^+$$

$$\frac{r_1}{8}CO_2 + r_1H^+ + r_1e^- \rightarrow \frac{r_1}{8}\,CH_4 + \frac{r_1}{4}H_2O$$

$$\frac{r_2}{2}\,CO_2 + r_2H^+ + r_2e^- \rightarrow \frac{r_2}{2}\,CO + \frac{r_2}{2}H_2O$$

$$r_3H^+ + r_3e^- \rightarrow \frac{r_3}{2}H_2$$

$r_4\ Imo\text{-}CH_3 + r_4\ e^- \rightarrow r_4\ Imo\text{-}CH_3^-$

Knowing the initial gas production rates R_{CO}, R_{CO2}, R_{CH4} and R_{H2} expressed in µmol.g^{-1}.h^{-1} (see Table 3 in the main text), we obtain the following solutions for the probabilities of the different chemical pathways:

$$r_1 = \frac{8R_{CH_4}}{X} - \frac{8(1-p)}{10}$$

$$r_2 = \frac{2R_{CO}}{X}$$

$$r_3 = \frac{2R_{H_2}}{X}$$

$$r_4 = 1\text{-}r_1\text{-}r_2\text{-}r_3$$

$$p = \frac{9}{4} - \frac{15}{2X}(R_{CO} + R_{CO_2} + R_{CH_4})$$

The last reduction pathway with a probability r_4 is written as the trapping of e$^-$ in the defects of Imo-CH_3 NTs. It could also be the reduction of traces of remaining dioxygen as discussed in the main text. However, it does not change the general validity of the equations.

Thus there exists a range of active electron/hole pair generation rates X (µmol.g^{-1}.h^{-1}) which satisfies these equations. Figure S7 represents the values of r_1, r_2, r_3, r_4 and p as a function of X.

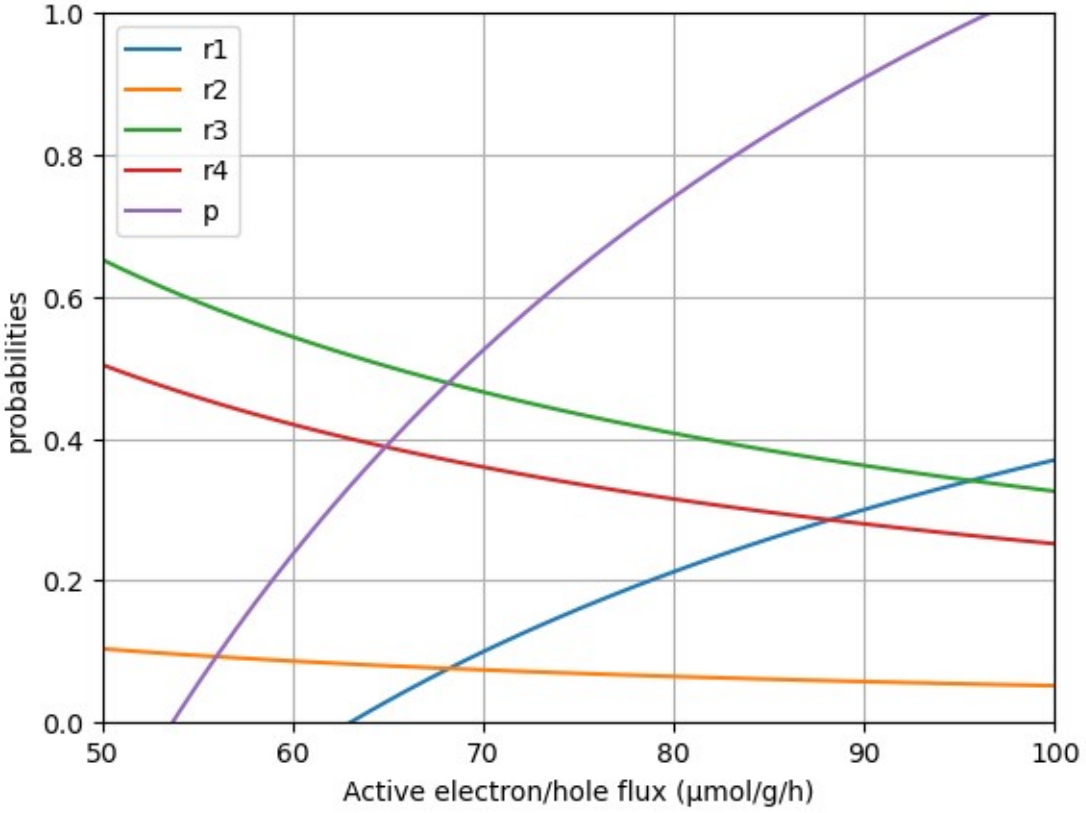

***F**igure S7. Probabilities p of oxidation according to reaction (R1) and of reduction pathways (r_1,r_2,r_3 and r_4) as a function of the active electrons/holes flux (*µmol.g^{-1}.h^{-1}*).*

10. Fluorescence emission spectra of Imo-CH_3 NTs in aqueous solution at different excitation wavelengths

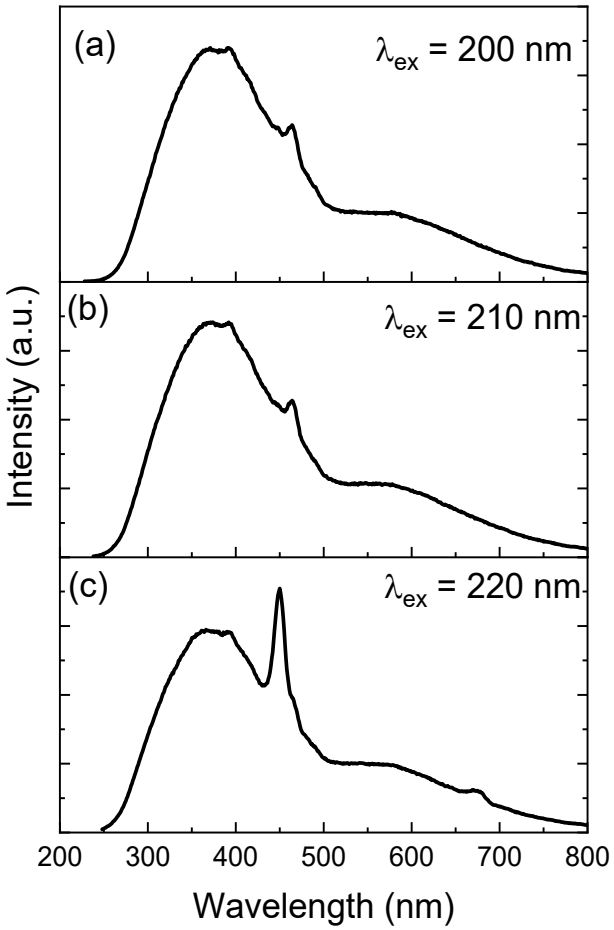

Figure S7. *Fluorescence emission spectra of Imo-CH_3 NTs in aqueous solution at different excitation wavelengths.*

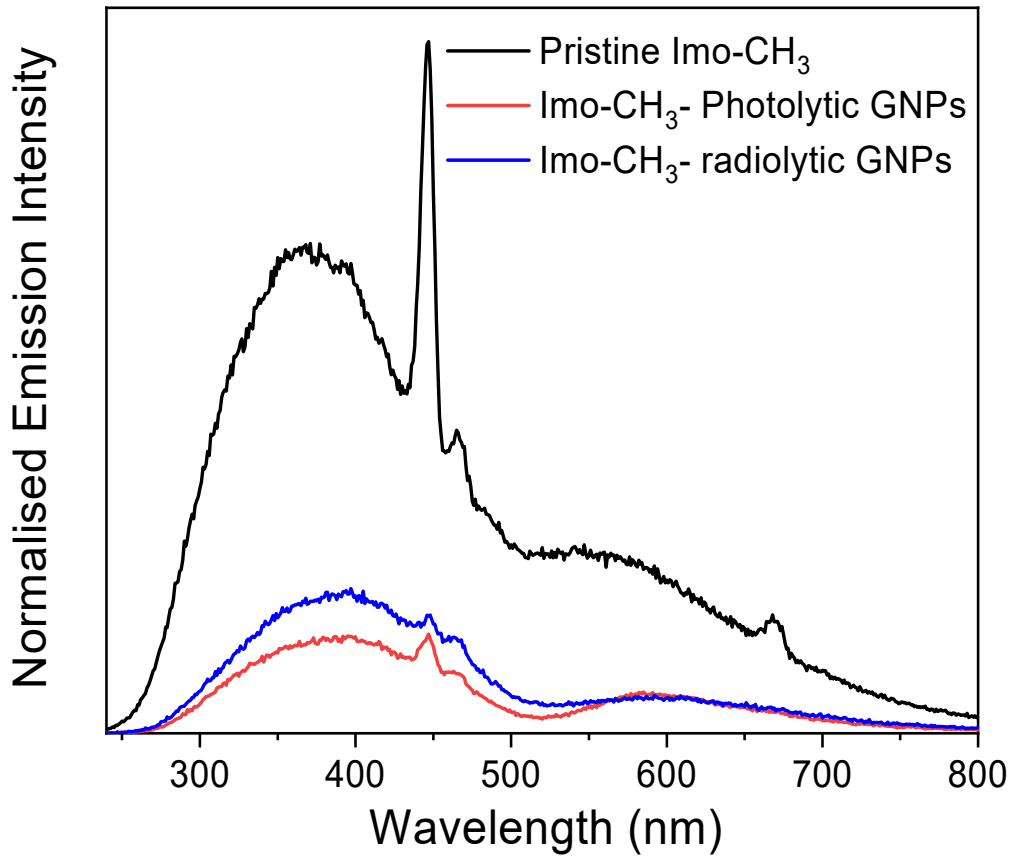

Figure S8. *Fluorescence emission spectra of pristine Imo-CH_3 and Imo-CH_3 coupled to GNPs prepared by UV photolysis and gamma radiolysis with an excitation at 220 nm. The emission intensities are normalized with respect to the UV-Vis absorbance at 220 nm.*

11. Gas Chromatography coupled to Mass Spectrometry (GC-MS) experiment

In order to identify the gases which could not be detected by µ-GC, a GC-MS experiment was performed for the photolytic GNP-Imo-CH_3 system after 6 h of UV illumination under an argon atmosphere. An Agilent 6890 GC instrument and an Agilent 5973 Mass Spectrometer were used. The mass spectrometer was equipped with an electron impact source, and a quadrupole mass analyzer. The mass range was 4-160. Helium was used as the vector gas with a flow rate of 2

mL.min^{-1}. Separation was carried out by two distinct separation modes: one with a CP-PorabondQ (25 m, Ø 0.32 mm) column (Varian), and on the other with a two-column system connected in parallel, a molecular sieve Rt-M Sieve 5 Å PLOT (30 m, Ø 0.53 mm) column (Restek) and a Rt-Q-PLOT (30 m, Ø 0.32 mm) column (Restek). The injector was set at 110°C in splitless mode. Figure S9 provides the GC-MS spectrum of the gases produced after 6h of UV illumination of a water/propan-2-ol (10 vol%) mixture in the presence of photolytically-produced GNP-coupled Imo-CH_3 NTs. Some small chain hydrocarbons along with ethanal and acetone were detected.

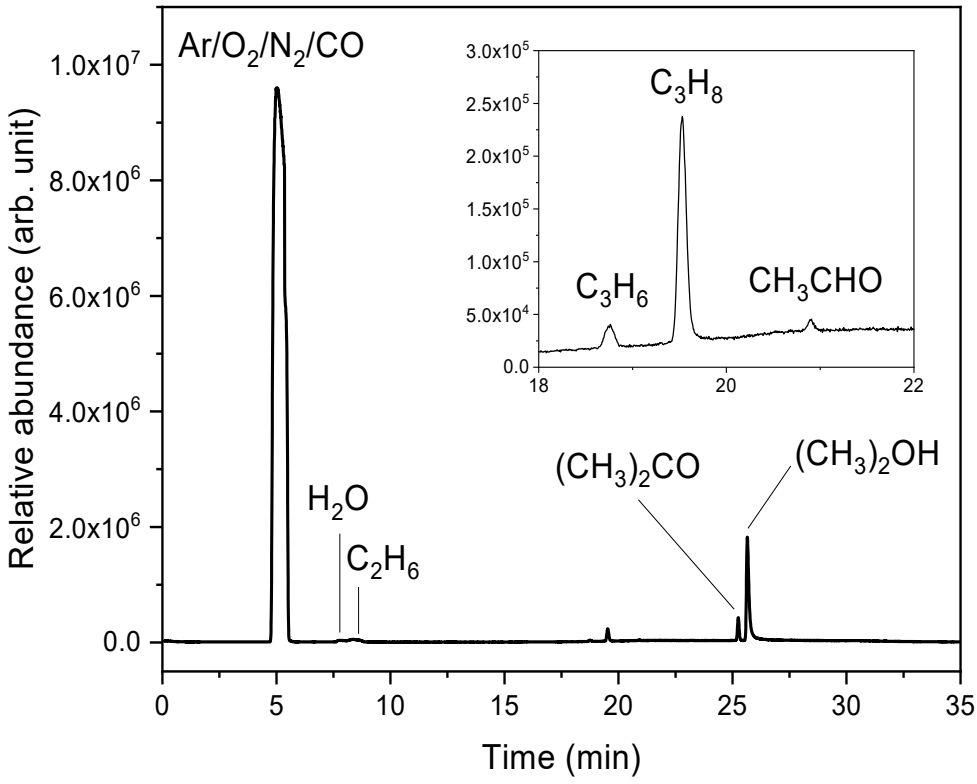

Figure S9. *GC-MS spectrum of the gases produced after 6h of UV illumination of a water/propan-2-ol (10 vol%) mixture in the presence of photolytically-produced GNP-coupled Imo-CH_3 NTs.*

References

1. O. Spalla, General Theorems in Small-Angle Scattering. In Neutrons, X-rays, and Light: Scattering Methods Applied to Soft Condensed Matter, T. Zemb, P. Lindner, Eds.; Elsevier: Amsterdam; Boston, 2002.

2. Y. Liao, P. Picot, J-B. Brubach, P. Roy, S. Le Caër, A. Thill, *Applied Clay Science,* 2018, **164**, 58-67.

3. S. Patra, D. Schaming, P. Picot, M-C. Pignié, J-B. Brubach, L. Sicard, S. Le Caër, A. Thill, *Environ. Sci.: Nano,* 2021, **8**, 2523-2541.